Experimental Evidence of Long-Lived Electric Fields of Ionic Liquid Bi-layers

Mattia Belotti[a], Xin Lyu[a], Longkun Xu[b], Peter Halat[c], Nadim Darwish[a], Debbie S. Silvester[a], Ching Goh[a], Ekaterina I. Izgorodina*[,c], Michelle L. Coote*[,b] and Simone Ciampi*[,a]

[a]School of Molecular and Life Sciences, Curtin University, Bentley, Western Australia 6102, Australia; Email: simone.ciampi@curtin.edu.au

[b]ARC Centre of Excellence for Electromaterials Science, Research School of Chemistry, Australian National University, Canberra, Australian Capital Territory 2601, Australia; Email: michelle.coote@anu.edu.au

[c]School of Chemistry, Monash University, Clayton, Victoria 3800, Australia; Email: katya.pas@monash.edu

ABSTRACT: Herein we demonstrate that ionic liquids can form long-lived double layers, generating electric fields detectable by straightforward open circuit potential (OCP) measurements. In imidazolium-based ionic liquids an external negative voltage pulse leads to an exceedingly stable near-surface dipolar layer, whose field manifests as long-lived (~1–100 h) discrete plateaus in OCP versus time traces. These plateaus occur within an ionic liquid-specific and sharp potential window, defining a simple experimental method to probe the onset of interfacial ordering phenomena, such as overscreening and crowding. Molecular dynamics modelling reveals that the OCP arises from the alignment of the individual ion dipoles to the external electric field pulse, with the magnitude of the resulting OCP correlated with the product of the projected dipole moment of cation with the ratio of predicted diffusion coefficient of cation and its volume. Our findings also reveal that a stable overscreened structure is more likely to form if the interface is first forced through crowding, possibly accounting for the scattered literature data on relaxation kinetics of near-surface structures in ionic liquids.

INTRODUCTION

Room-temperature ionic liquids (RTILs) are liquids with melting points below 25 ºC, composed solely of anions and cations.[1-2] They have been known for over a century,[3] but entered mainstream electrochemical research only in the middle of the 1990s, with the discovery of RTILs with stable anions.[4] Several such RTILs are now commercially available, and unlike conventional solvent-based electrolytes they can have exceedingly large electrochemical windows.[1, 4-5] This makes them valuable in applications ranging from energy generation and storage, to electrocatalysis.[6-9]

RTILs are typically comprised of large unsymmetrical ions[10] that form what can be approximated as a coordinated network of ions,[11-12] with intermolecular forces tunable through changes in the molecular structure of the ions.[13-14] The unique nature of RTILs has important implications for the structure and dynamics of their interface with solid electrodes. While large molecular sizes and conformational flexibility prevent the formation of an ordered solid in the bulk,[15] RTILs at interfaces are inherently ordered.[16] Specifically, RTIL double-layer structures[17-19] formed in the proximity of charged electrodes are of great practical importance as this phase boundary governs charge transport, energy storage and lubricating properties of electrode–RTIL systems.[9, 20-21] As the electrode is charged away from its potential of zero charge (PZC hereafter) in response to an external bias, counterions are enriched in a first ionic layer, where their lateral diffusivity is lower than in bulk.[22] This charged first layer induces a second ionic layer of opposite charges, and so on, causing the potential profile to decay with damped oscillations.

Despite a general consensus on the presence of an alternating out-of-plane arrangement of cation- and anion-rich layers,[23-24] the exact short-range ordering of RTILs near electrodes remains unclear.[16, 25-28] To date, experimental insights on the interface between RTILs and electrodes have relied on technically demanding atomic force microscopy,[24, 29] X-ray reflectometry (XRR) experiments and Raman spectroscopy.[17, 30] The lack of routine and straightforward measurements, suitable to probe the electrode–ionic liquid interface, is part of the reason why details of the near-electrode structure are still unclear. In the present work we address this problem by introducing open-circuit potentiometry as a rapid and technically simple method to probe the interface between RTILs and electrodes.

Firstly, quantitative data on RTIL double layer dynamics, as well as data on the magnitude of the potential required to trigger the formation of ordered layers, are scattered. While solvation dynamics of bulk RTILs have a time scale between picoseconds and nanoseconds,[31] the relaxation of RTILs at interfaces is significantly slower.[32-35] But how slow is unclear, with available data indicating relaxation times varying between a few seconds to several minutes.[32, 35]

Secondly, while some authors argue that at potentials close to the PZC counter-ions will already overscreen electrode charges,[26, 36] others advocate for such features occurring only at larger biases and persisting over large potential windows.[37-39] For instance Yamamoto and co-workers put forward data in favour of RTILs over-screening at biases around +1.5 V,[18] while

Uysal and co-workers observed this already at −0.4 V.[40] Moreover, there is also the hypothesis of electrode "crowding" at large anodic and cathodic excursions,[26, 41] as well as a debate around whether the thickness of the first ionic layer drops with increasing electrode charges,[42-44] or whether it remains essentially unchanged.[45] Addressing these issues is important because the phase boundary ultimately governs how energy is stored in the electric field of electrochemical devices, such as capacitors,[9, 46-47] and how accessible the electrode surface is towards charge-transfer reactions. The latter is emerging as a viable strategy for controlling the balance between inner- and outer-sphere competing electron transfer reactions, both for electrocatalysis and electrosynthesis.[48-49] Moreover, recent computational work has shown that ionic liquids that are ordered as a result of exposure to external electric fields can generate strong internal electric fields that electrostatically catalyze chemical reactions, even when the external field is removed.[50] Experimental confirmation of these fields, and measurements of their lifetime, would be the first step toward harnessing these electrostatic effects in chemical synthesis.[51-54]

By means of open-circuit potentiometry we demonstrate that at electrode surfaces RTILs assume stable ordered structures, and generate significant endogenous electric fields that persist for days after an external potential is removed.

RESULTS AND DISCUSSSION

Interfacial Dynamics of [EMIM][EtSO4]. Prior to studying the response of RTILs to an applied potential, we conducted a search of the minimum of the electrode–RTIL capacitance as a function of the electrode potential. This minimum provides a baseline reading for the disordered RTILs against which the ordered RTILs could be compared, and it was obtained through electrochemical impedance spectroscopy (EIS). The potential where capacitance reaches a minimum generally coincides with the electrode PZC,[43] and EIS measurements with platinum electrodes indicate that this is close to −0.6 V vs Fc/Fc^+ (Figure 1a). The accumulation of counter-ions at the electrode surface is likely to occur in both bias directions,[27] implying that the positive and negative branches of the capacitance–potential curve around the PZC are delimiting bias regions where the liquid side of the interface is enriched of either anions or cations.

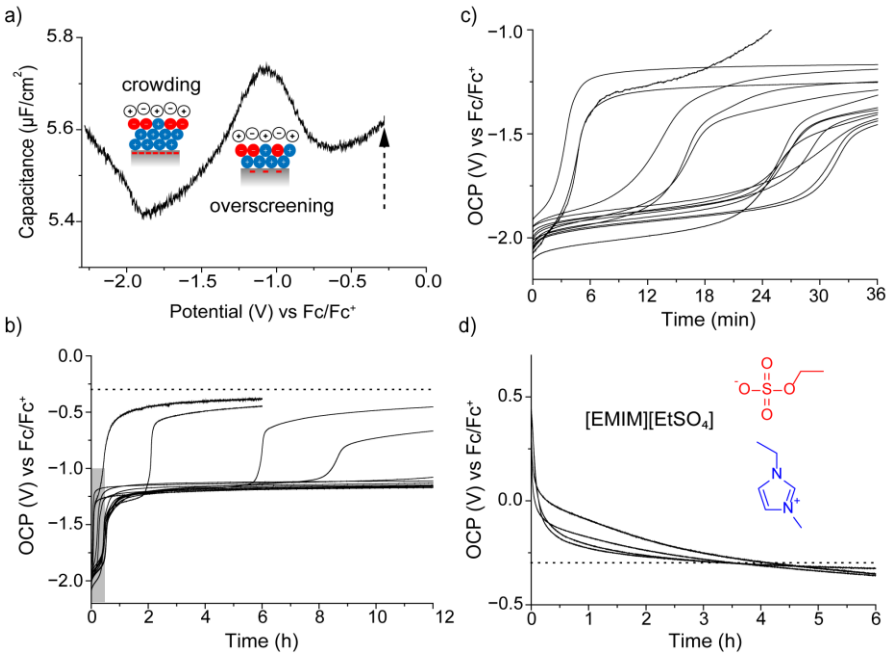

Figure 1. (a) Representative electrochemical impedance spectroscopy (EIS) capacitance–potential plot, with a schematic depiction of the onset of overscreening and crowding in correspondence of local capacitance maximum and minimum, respectively (platinum disk in [EMIM][$EtSO_4$]). The vertical arrow indicates the system initial OCP value, prior to any external biasing. Representative OCP–time measurements for platinum electrodes immersed in [EMIM][$EtSO_4$] recorded after the application of negative (b,c), and positive (d) potential steps (60 s, ±2.0 V relative to the initial OCP). Dotted horizontal lines represent the average initial OCP. (b) Negative bias excursions lead to very stable OCP plateaus located between −1.1 V and −1.3 V vs Fc/Fc^+. (c) A relatively short-lived and more negative OCP plateau, found between −1.9 V and −2.0 V, is evident upon close inspection of the first 30 minutes of the OCP relaxation data. The grey shaded area in (b) indicates the data region shown in (c).

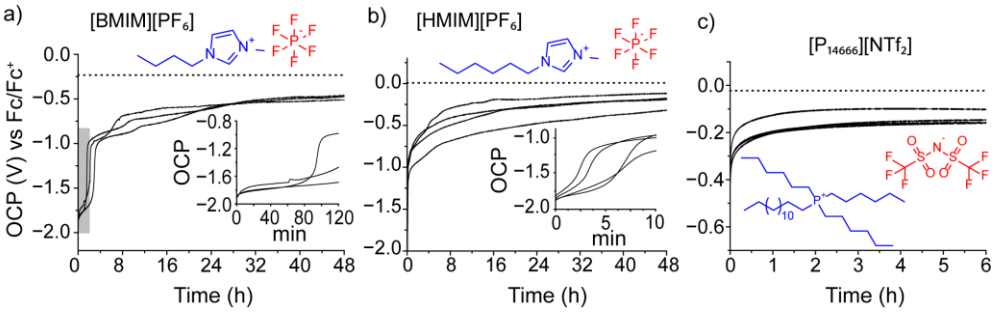

Figure 2. Representative OCP–time measurements acquired with platinum electrodes immersed in [BMIM][PF_6] (a), [HMIM][PF_6] (b), and in [P_{14666}] [NTf_2] (c) after a negative potential step (60 s). The potential step was of −2 V away from the electrode initial rest OCP (dotted horizontal lines). The grey shaded areas in (a,b) indicate the data plotted as figure insets. Data in (a) reveal the onset of crowding in [BMIM][PF_6] as an OCP vertical step located between −1.7 V and −1.8 V. The overscreening OCP signature is found between −0.9 V and −1.0 V. (b) OCP–time data for [HMIM][PF_6] with evidence of discernible OCP plateaus at ~−1.7 V and poorly defined plateaus between −1.0 V and −0.75 V.

Prior to exposure to an applied potential, the rest open circuit potential (OCP) was generally only slightly positive of the PZC. After a short (60 s) potential step, equal or smaller than ±1.0 V away from this initial OCP (dashed arrow and dashed horizontal lines in Figure 1) we were only able to record a rapid, <30 minutes, equilibration of the electrode potential back to its initial rest value (Supporting Information, Figure S1). In this respect an electrode–RTIL interface, such as platinum immersed in [EMIM][$EtSO_4$], behaves qualitatively similar to the interface formed between electrodes and conventional molecular solvent-based electrolytes, such as Bu_4NClO_4 in acetonitrile (Supporting Information, Figure S2). Surprisingly, the experimental OCP relaxation was rapid despite the magnitude of the cathodic step (−1.0 V) being more than sufficient for the interface to reach its capacitance maximum (~−1.1 V vs Fc/Fc^+, Figure 1a). It is therefore probable that the −1.0 V step triggered the formation of an ordered overscreened interface,[41, 55] but this structure did not persist once the external bias was removed. As ordering will progressively increase with bias,[18] and since capacitance drops under fully occupied conditions, [23] the presence of a minimum in the negative branch of the capacitance–potential curve at ~−1.9 V vs Fc/Fc^+ (Figure 1a) suggests the possibility of a thicker first layer of counter-ions forming at this more negative bias. We consequently measured the OCP relaxation that followed a cathodic step of −1.5 V from the initial rest potential. Once again, this bias is sufficient for the system to reach the capacitance minimum (crowding), but OCPs still relaxed asymptotically and very slowly (~3 h).

A remarkably different response was observed when the electrode potential was disturbed away from its rest potential by a potential step as large as −2.0 V. Applying such a large negative pulse was effective in locking the interface in a stable 'cation-rich' configuration. This cation-rich ordered configuration manifested as an OCP plateau between −1.1 V and −1.3 V vs Fc/Fc^+, which persisted rarely less than 6 h (Figure 1b), and occasionally up to four days (Supporting Information, Figures S3–S6). Importantly, the position of these long-lived OCP plateaus matches the onset of overscreening as assessed by EIS (Figure 1a). A closer inspection of the first part of the time-resolved OCP measurements revealed the consistent presence of a more negative plateau between −1.9 V and −2.0 V (Figure 1c). The position of this initial plateau closely matches the onset of crowding in the EIS data (Figure 1a). These initial cation-rich surface structures persist only for short times, from few seconds to ~30 minutes, which is of the same order of magnitude of relaxation times obtained for ionic liquid systems through much more complex techniques.[32, 40]

Chemisorption reactions, potentially triggered by the cathodic pulse, are an unlikely cause for the plateaus. For instance, while very gentle vibrations of the electrochemical cell did not disturb an overescreening OCP plateau, extracting and re-immersing the electrode in the liquid was enough to reset the initial OCP (Supporting Information, Figure S6). Molecules chemisorbed on surfaces are not so easily removed.[56] Further evidence against chemisorption is the lack of a change in electrode active area following the pulse (Supporting Information, Figure S7).

The existence of such negative plateaus is in accordance with the theory of Kornyshev and co-workers, where multiple layers of counter-ions balance surface charges (see schematics in Figure 1a).[26, 57] Interestingly, only when the metal charge density has sufficiently decreased, the double layer can then adjust to an overscreening organization, where just a monolayer of counter-ions balances the surface charge (Figure 1a). In brief, implicit from our data is that a stable overscreened arrangement forms if the system is first forced into crowding. On the other hand, OCP relaxation responses following positive potential steps were featureless: no plateaus were detected and OCPs relaxed asymptotically (Figure 1d). A similar conclusion was previously reached by AFM data, where the force required for an AFM tip to push through the first ionic liquid layer was significantly larger for negative biases.[27, 45] It was therefore not surprising that the occurrence of these negative OCP signatures was largely independent of the nature of the anion, with for instance [EMIM][$EtSO_4$] behaving very similarly to [EMIM][BF_4] (Supporting Information, Figure S8). We have not tested [EMIM][PF_6], because, in spite of its commercial availability, it is not liquid at room temperature.

Comparison of Different RTILs. To define the generality of OCP measurements in probing interfacial dynamics we then

proceeded to test a range of RTILs with different cations. Imidazolium cations with longer alkyl side chains have higher permanent dipole moments, and this in turn increases the strength of their electrostatic interaction with the applied electric field. To illustrate this trend experimentally, we measured OCP relaxations in RTILs containing butyl and hexyl substituents on the imidazolium ring. Data in Figure 2a,b show that after an anodic step the relaxation behavior of [BMIM][PF_6] and [HMIM][PF_6] is asymptotic and indistinguishable to that of the smaller [EMIM][$EtSO_4$] in Figure 1d. After a cathodic excursion, both [BMIM][PF_6] and [HMIM][PF_6] form negative plateaus, but especially in the case of [HMIM][PF_6], these OCP signatures are not as long-lived and well-defined as those observed with [EMIM][$EtSO_4$] (Figure 2a,b). OCP signatures for overscreening are still clearly visible for both [BMIM][PF_6] and [HMIM][PF_6], although shorter in the latter (insets in Figure 2). Crowding features in the OCP–time plot are clearly distinguishable only for [BMIM][PF_6]. Extending the duration of the cathodic step, from one to six minutes, did not alter the dynamics of the OCP relaxation (Supporting Information, Figure S9). The ability to form ordered dipolar structures disappears for larger cations, such as for example with [P_{14666}][NTf_2] (Figure 2c), and despite previous reports suggesting that a more localized charge leads to stronger surface interactions,[58] pyrrolidinium-based RTILs did not generate clear OCP signatures ([BMPyrr][NTf_2], Supporting Information, Figure S10).

Effect of Electrode Material. There is also experimental evidence of a relationship between ordering on the liquid side of the interface and the mobility of surface atoms of the electronic conductor. Similarly to platinum, OCP plateaus were also observed on gold surfaces, but surprisingly they were not detected on covalent electrode materials of large self-diffusion activation energy,[59] such as silicon and carbon (Supporting Information, Figures S11–S13). Further, plateaus recorded with gold electrodes were located at less negative voltages than for platinum, between −0.6 V and −0.7 V, an observation for which we do not yet have a satisfactory explanation (Supporting Information, Figure S14). Differences in double-layer structures for a given RTIL between platinum and gold are not unprecedented,[60] but at present we can only speculate that a less negative OCP plateau for ordered dipolar structures on gold may relate to a difference in surface diffusivity between the two metals.[61]

Polarizable Molecular Dynamics Studies. To understand these results, we conducted polarizable molecular dynamics [39] simulations for [BMIM][PF_6], [EMIM][$EtSO_4$], and [HMIM][PF_6] in the presence and absence of an applied electric field of 0.2 V/Å along the z-axis. Imidazolium-based ionic liquids are known to exhibit strong hydrogen bonding between the C_2–H bond on the imidazolium ring and electronegative atom on the anions.[62] Radial distribution functions (RDFs, Figures 3a and 3c) of the (C_2)H···F interionic distances indicate the significant changes in the short and long-range order of both PF_6-based ionic liquids upon the application of the electric field. [EMIM][$EtSO_4$] and [BMIM][NTf_2] demonstrated smaller structural changes in the (C_2)H···O interionic distances (Figures 3e and 3g), suggesting that the constituent ions do not require a significant change in the bulk arrangement to align with the electric field. Angular distribution functions (ADFs) of the C_2–H···X bond (where X is either F (PF_6^-) or O ($EtSO_4^-$ and NTf_2^-; Figures 3b, 3d, 3f and 3h) clearly identify that the hydrogen bond in all three ionic liquids undergoes a change from a more directional hydrogen-bond type (a peak at 130°) to a non-directional interaction above the imidazolium ring (a peak at 55°). The occurrence of the latter strongly suggests that ionic liquid ions re-align themselves in the electric field. Some anions become located right above the imidazolium ring, which corresponds to a typical interionic interaction mode in these ILs.

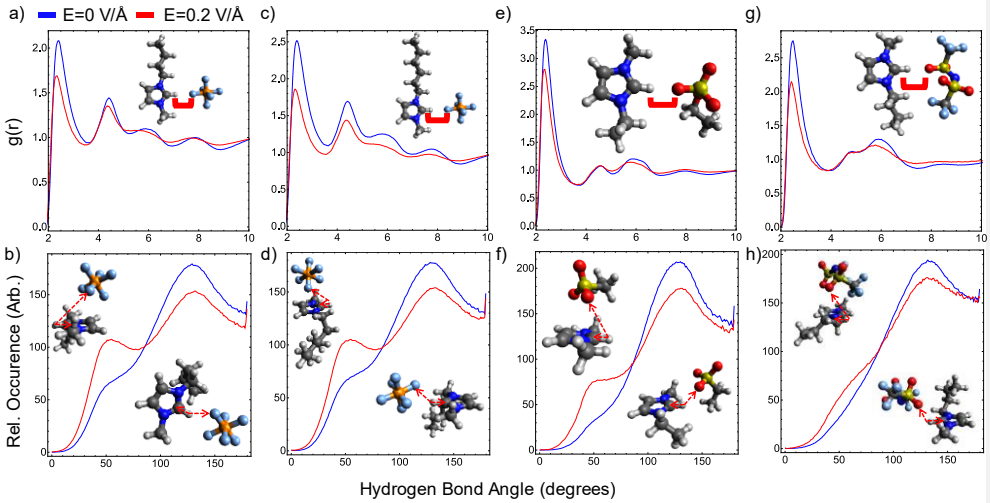

Figure 3. Normalized radial distribution functions of (C_2)H–F distances in (a) [BMIM][PF_6] and (c) [BMIM][PF_6] and (C_2)H–O distances in (e) [EMIM][$EtSO_4$] and (g) [BMIM][NTf_2]. Cone-corrected angular distribution functions of C_2–H–F angles in (b) [BMIM][PF_6] and (d) [HMIM][PF_6] and C_2–H–O distances in (f) [EMIM][$EtSO_4$] and (h) [BMIM][NTf_2]. In all panels, blue lines denote behavior without an external field, and red lines denote behavior in an external 0.2 V/Å field. Insets in (b), (d), (f) and (h) are motifs representative of the two main peaks at 55° and 130°.

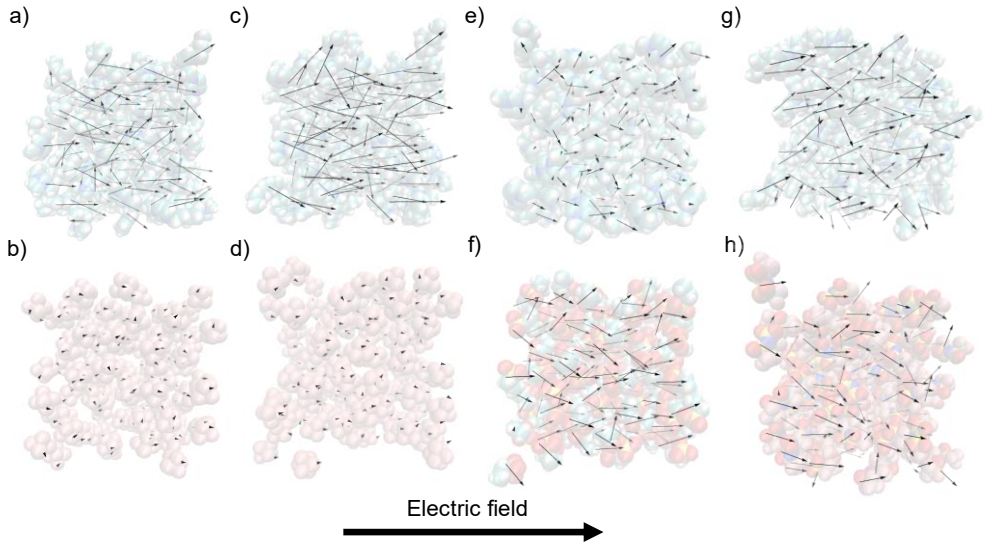

Figure 4. Visualizations of dipole moments of ions (a) $BMIM^+$ and (b) PF_6^- in [BMIM][PF_6], (c) $HMIM^+$ and (d) PF_6^- in [HMIM][PF_6], (e) $EMIM^+$ and (f) $EtSO_4^-$ in [EMIM][$EtSO_4$] and (g) $BMIM^+$ and (h) NTf_2^- in [BMIM][NTf_2] under a 0.2 V/Å electric field in molecular dynamics simulations. Dipole vector lengths are calibrated to 1 Å/D.

The strong alignment of the ion dipole moments with the field is presented in Figure 4. Ion dipole moments were calculated with centre-of-mass reference points, with magnitudes equivalent to the 'charge arm' calculated with respect to center of charge.[63-64] The alignment is particularly stark for ions with non-zero dipole moments such as the imidazolium cations, $EMIM^+$, $BMIM^+$ and $HMIM^+$, and the $EtSO_4^-$ and NTf_2^- anions. The PF_6^- anion that does not have a nominal dipole moment, when calculated in isolation, becomes strongly polarized in the presence of other ions, with the dipole moment also becoming aligned in the field. The alignment of the individual ion dipole moments is not perfect due to strong intermolecular interactions between ionic liquid ions in the range of 320 to 420 kJ mol^{-1} per single ion pair.[65] The deviation from the field direction was estimated by calculating the average θ angle between the apparent dipole moment of each ion and the direction of the field (Figures 5a and 5b). It is not surprising and rather reassuring that, in the absence of the electric field, the average θ value was observed to be ~90° for all ions. This indicates a random distribution, with cone-corrected angular distributions in the Supplementary Information (Figure S15) serving as further proof.

The situation changes dramatically as the field is introduced, with the average θ value falling between 35.6° for $EtSO_4^-$ and 49.4° for $EMIM^+$. Further analysis reveals that θ only weakly correlates with the dipole moment of the ions, smaller θ values loosely corresponding to larger dipole moments. In addition to the dipole orientation, each ion dipole moment was projected along the external field axis, μ_z, (Figures 5c and 5d). All ions besides PF_6^- exhibit a strong projection ranging from 2.24 D for $EMIM^+$ to 9.82 D for $HMIM^+$. This is due to the strong permanent dipole moments present in the imidazolium cations, the $EtSO_4^-$ and the NTf_2^-, whereas the PF_6^- anion does not have a permanent dipole moment due to symmetry. The projected induced dipole moment of PF_6^- anions is not negligible, averaging 0.53 D for both [BMIM][PF_6] and [HMIM][PF_6].

The alignment of these ion dipoles to the applied electric field induces an opposing internal electric field that, we hypothesize, is responsible for the OCP observed when the external field is removed. The process of the ion re-alignment is also accompanied by cations moving to the anode and anions moving to the cathode. In our MD simulations diffusion coefficients of cations and anions increased by four orders of magnitude on average when the field was applied (see Supporting Information, Tables S3 and S4). $BMIM^+$ and $HMIM^+$ cations in the PF_6-based ionic liquids were found to diffuse slightly faster than cations in [EMIM][$EtSO_4$] and [BMIM][NTf_2], which can be explained by stronger hydrogen bonding preventing ions from moving freely in the latter. We also confirmed that the NTf_2^- anion maintained its *trans* configuration throughout the entire simulation in an external electric field (Supporting Information, Figure S16). The calculated diffusion coefficients, ranging from 3.7×10^{-7} to 2.5×10^{-6} $m^2 s^{-1}$, suggest that ions can easily move to electrodes, thus leading to crowding of cations at the anode as shown in Figure 1a. It was also noticed that the mobility of cations correlated with the projected dipole moment and the strength of intermolecular interactions within an ionic liquid. The ability of cations with a larger dipole moment and weak hydrogen bonding to anions to strongly re-align with an electric field is reflected in their increased diffusion coefficient.

Since ions of opposite charge move in opposite directions in an electric field, it is not surprising that the projected dipole moment sum of the cation and anion did not correlate with the

Commented [DS1]: Just checking if this is correct, as usually cations (positively charged) move to the cathode (negatively charged). Unless this means they are moving when the external field is removed?

Commented [SC2]: Katya, here you are talking of the alignment in response to the external field or of the relaxation once the field is removed? (also, the "re" alignment is causing a bit of confusion. Maybe just "alignment"?
If it is the first, then we should say "cations moving towards the cathode", if we talk instead of relaxation once the bias is removed, then we can say "cations diffusing away from what was the negative electrode".
Or we can perhaps even remove this entire sentence.

Commented [EP3R2]: I what we need to add is re-alignment of their dipole moment with the direction of the field. What I also mean here is that cations will not only realign in the field but also move towards the negatively charged electrode. I suggest that we use the terminology of negatively and positively charge electrodes instead of anode and cathode to avoid any confusion! How about this:
"The process of the re-alignment of the ion's dipole moment with the direction of the field is also accompanied by cations moving towards the negatively charged electrode and anions moving towards the positively charged electrode under bias potential."

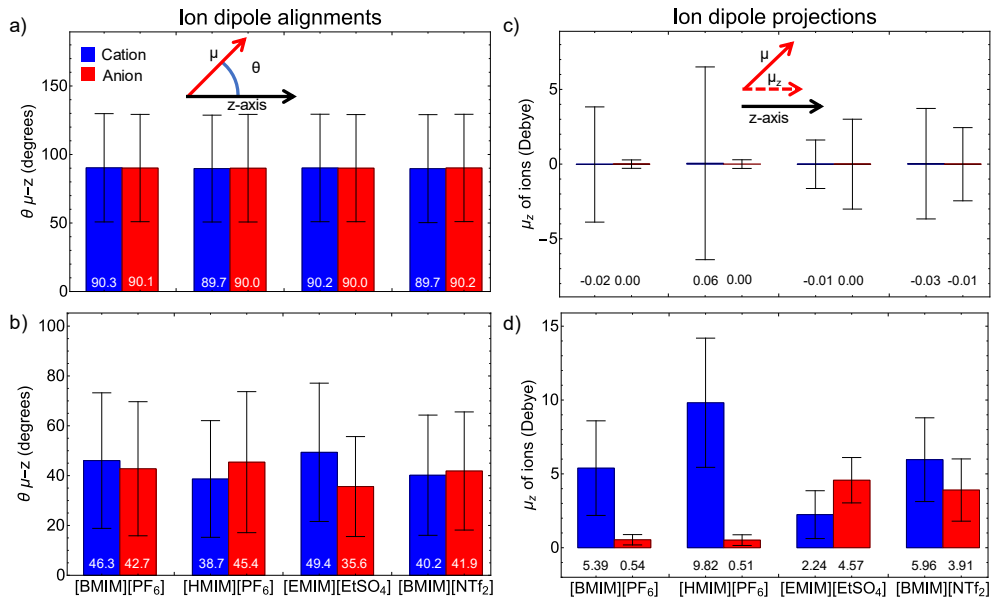

Figure 5. Average angles between ionic dipole moments and the z-axis (a) without an external electric field and (b) in an external field of 0.2 V/Å along the z-axis. Panel (c) displays mean ion dipole projections along the z-axis without an external electric field, and (d) in an external field of 0.2 V/Å oriented along the z-axis. Error bars in (a)–(d) represent standard deviations.

experimental OCP plateaus (Supporting Information, Figure S17). It is well known that cations will form a crowding layer next to the cathode, thus creating a medium of different viscosity at the interface compared to that of the bulk of an ionic liquid. The density of coverage also depends on the cation size, with larger cations creating less dense coverage. Therefore, it was hypothesized that the average projected dipole moment of cation corrected for changed viscosity at the electrode interface and cation size should correlate with the OCP. Since viscosity is inversely proportional to diffusion coefficient, the product of the projected dipole moment of cation with the ratio of predicted diffusion coefficient of cation and its volume gives a strong correlation to the observed OCP plateaus (Figure 6) with an R^2 of 0.907.

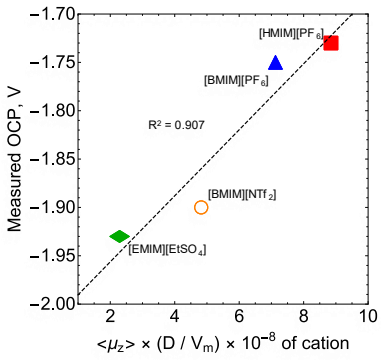

Figure 6. Correlation of measured OCP values (crowding) of ionic liquids against the product of average dipole moment projections and diffusion coefficients in the electric field, divided by cation molar volumes.

This correlation suggests that the mobility of cations in an electric field plays a key role in the formation of a stable crowding interface ~~at the anode~~ resulting in negative OCP plateaus. Lower mobility of $EMIM^+$ and $BMIM^+$ in an electric field in ionic liquids with strong hydrogen bonding, reflected in small structural changes, allows for cations to form a more stable crowding interface, thus exhibiting the lower OCP plateaus (Figures 1c and S18, Supporting Information). This conclusion is further reinforced by the absence of a clear plateau in $[P_{14666}][NTf_2]$ (Figure 2c), in which the cation displays a negligible dipole moment and hence, very low mobility.[63, 66] The presented MD simulations thus confirmed that ionic liquid ions are able to reorient their dipole moments along the external electric field without sacrificing their bulk structure to a great extent.

CONCLUSIONS

We have described a simple and straightforward method to detect order and electric fields of organized and long-lived ionic liquid double layers by open circuit potentiometry. We show that overscreened and crowded near-electrode structures are detectable as negative open-circuit signatures occurring within sharp potential windows, validating ionic liquids double layer models proposed by Kornyshev and co-workers.[26] Crowding

Commented [EP4]: I think that the use of cathode is correct here. For clarity we could say "next to the cathode, the negatively charged electrode under bias potential)."

Commented [EP5]: I would say "the electrode interface"

Commented [EP6]: I am happy with this change.

Commented [DS7]: Here again

manifests as negative OCP plateaus, which survive up to several tens of minutes. This structure rearranges into an over-screened double layer, lasting up to several days, where just a monolayer of counter-ions balances the surface charge. These fields can potentially be harnessed for the electrostatic catalysis of chemical reactions,[50, 67-68] for the development of safe supercapacitors, and can find applications in the emerging field of redox-enhanced electrochemical capacitors.[69-70] The presence of a stable blocking layer on the electrode may limit side reactions in electrosynthesis, such as reducing hydrogen evolution in the presence of trace water. Further, slow double layer dynamics in RTILs are known to manifest in voltammetry,[32] and to introduce hysteresis in capacitance measurements[34]; here we show that RTILs forming dense dielectric layers can be rapidly identified by OCP measurements.

Polarisable molecular dynamics simulations demonstrated the loss of short- and long-range order in [BMIM][PF_6], [HMIM][PF_6] and to a lesser extent, [EMIM][$EtSO_4$] and [BMIM][NTf_2] under an external electric field. The ionic liquid ions were confirmed to align their dipole moments with the external field. The alignment of ions was found to depend on presence of strong hydrogen bonding in ionic liquids. Cations with larger projected dipole moments were also found to have increased mobility in an electric field. The projected dipole moment of the cation, corrected for its volume and mobility in an electric field, correlate well with the observed crowding OCP plateaus, suggesting that increased dipole moment strength and mobility prevent cations from forming a more stable crowding interface. This represents an excellent design parameter to predict the likelihood of forming stable ionic liquid bilayers having strong endogenous electric fields.

EXPERIMENTAL SECTION

Materials. Unless noted otherwise, all reagents were of analytical grade and utilized without further purification. Milli-Q™ water (>18.2 MΩ cm) was used for cleaning procedures and to prepare electrolytic solutions. 1-Ethyl-3-methylimidazolium ethyl sulfate (≥95%, Sigma, [EMIM][$EtSO_4$]), 1-butyl-3-methylimidazolium hexafluorophosphate (≥97% Sigma, [BMIM][PF_6]), 1-hexyl-3-methylimidazolium hexafluorophosphate (≥97%, Sigma, [HMIM][PF_6]), trihexyltetradecylphosphonium bis(trifluoromethylsulfonyl)imide (>98%, Iolitec, Germany, [P_{14666}] [NTf_2]), 1-butyl-1-methylpyrrolidinium bis(trifluoromethylsulfonyl)imide (99.5%, Iolitec, Germany, [BMPyrr][NTf_2]), 1-ethyl-3-methylimidazolium tetrafluoroborate (>98%, Iolitec, Germany, [EMIM][BF_4]), 1-butyl-3-methylimidazolium bis(trifluoromethylsulfonyl)imide (99%, Iolitec, Germany, [BMIM][NTf_2]), acetonitrile (99.5%, VWR chemicals, USA, MeCN) and tetrabutylammonium perchlorate (≥98%, Sigma, Bu_4NClO_4) were used as received. The water content of all the ionic liquids used in this work was estimated by Karl Fisher titration (Mettler-Toledo C20S Compact Coulometer, Honeywell HYDRANAL™ Coulomat AG reagent, Merck Water Standard 0.1%, USA), and with at least three samples measured for each ionic liquid. The water content readings between samples of the same ionic liquid varied less than 50 ppm, and the average values were: [EMIM][$EtSO_4$], 930 ppm; [EMIM][BF_4], 500 ppm; [BMIM][PF_6], 490 ppm; [HMIM][PF_6], 745 ppm; [BMPyrr][NTf_2], 125 ppm; [P_{14666}][NTf_2], 1215 ppm; [BMIM][NTf_2], 100 ppm.

Electrochemical Methods. All electrochemical measurements were carried out using a small (~4 mL) single-compartment three-electrode glass cell. Cyclic voltammetry (CV) and open circuit potentiometry (OCP) experiments were performed on an Emstat3 Blue potentiostat (PalmSens BV, Houten, Netherlands). Electrochemical impedance spectroscopy (EIS) experiments were carried out using a CH 650D electrochemical analyser (CH Instruments, Austin, USA), imposing an AC potential amplitude of 15 mV (root mean square) over the DC offset (E_{dc}) of the working electrode. The AC frequency was varied between 0.1 Hz and 0.1 MHz. Reproducibility of the EIS data was highest at 1 kHz, as also observed by others,[43, 71-72] and therefore capacitance–voltage data in this work refer only to this frequency. The E_{dc} offset of the working electrode was ramped starting from the system's initial OCP and moved towards the cathodic limit of the sweep. The sweep rate was 40 mV/s. This sampling approach is common practice for EIS experiments in molten salts.[73] The out-of-phase impedance (Z'') was used to estimate the electrode capacitance ($C = 1/(\omega Z'')^{-1}$). For all the electrochemical experiments the cell was loaded with a small sample (10 mL) of the ionic liquid, which was previous degassed by means of bubbling it with high-purity argon gas (99.997%, Coregas) for at least 20 min. Platinum wire was used as working and counter electrode for both CV and OCP experiments (0.5 mm diameter wire, 99.99+%, Goodfellow Cambridge Limited), while EIS data were recorded at platinum disk electrodes (eDAQ, ET052, 3 mm diameter). The size of the counter electrode was in excess of twenty times that of the working electrode. A plastic body silver/silver chloride "leakless" setup was used as the reference electrode (eDAQ, part ET072-1, 3.4 M aqueous potassium chloride as filling solution). The active area of the platinum wire working electrodes was either 0.28 cm^2 or 0.63 cm^2, as determined from the refinement of a E model (DigiElch-Professional v7, ElchSoft) against experimental voltammogramms measured in 1.0×10^{-1} M MeCN/Bu_4NClO_4 and in the presence of 1.0×10^{-3} M of ferrocene (Fc in shorthand hereafter, Supporting Information, Figures S19 and S20). The active surface area of the platinum disk was 0.08 cm^2 (Supporting Information, Figure S21). The size of the working electrode had no measurable effect on the OCP versus time results. The reference electrode was calibrated before and after each experiment against the apparent formal potential of the ferrocene/ferricenium couple (Fc/Fc^+) measured with the platinum disk using 1.0×10^{-3} M Fc in 2.0×10^{-1} M MeCN/Bu_4NClO_4, and unless specified otherwise potentials are reported against the Fc/Fc^+ couple. Electrochemical experiments were performed at room temperature (23 ± 2 °C) inside a gas-tight acrylate box (Molecular Imaging, model GB306, USA) kept under nitrogen atmosphere. The nitrogen line was fitted with a Drierite™ gas drying unit (Sigma). Working and counter platinum electrodes were cleaned prior to the experiments by means of multiple cyclic voltammetry scans in aqueous 0.5 M sulfuric acid, ramping the potential between −0.2 and 1.0 V at a voltage sweep rate of 0.05 V s^{-1}. Control experiments with gold, carbon and silicon surfaces were done using, respectively, gold wire of 0.25 mm diameter (99.999+%, Goodfellow), glassy carbon plates of 12.7 mm diameter (TED PELLA, Inc.), and highly doped monolayer-coated oxide-free silicon wafers (prime grade, CZ, 111-oriented (± 0.5°), 500 µm thick, single-side polished, boron-doped, 0.007–0.013 Ω cm, from Siltronix, S.A.S, Archamps, France). The gold wire was cleaned prior to the experiments by means of cyclic voltammetry in aqueous 50 mM sulphuric acid (sweeps in the –0.2 to 1.0 V range, at 0.05 V s^{-1}). Glassy carbon electrodes were polished

to mirror-like finish with alumina slurry (0.05 μm, eDAQ, ET033) on a polishing cloth (Struers). After the polishing step, the electrodes were sonicated in water for one minute.

Hydrogen-terminated silicon electrodes were modified with an organic monolayer of 1,8-nonadiyne (98%, Sigma-Aldrich) in order to passivate the oxide-free surface against anodic decomposition. The procedure follows minor modification of literature procedures.[74-76] In brief, silicon wafers (1 × 1 cm) were kept for 30 min in piranha solution (100 °C, a 3:1 (v/v) mixture of concentrated sulfuric acid and 30 % hydrogen peroxide), then rinsed with water, and etched for 10 min in deoxygenated aqueous ammonium fluoride (40 wt. %). A small amount of ammonium sulfite was added to the etching solution as oxygen scavenger. Hydrogen-terminated silicon samples were then rinsed with water, dichloromethane, dried under a flow of nitrogen, and then covered with a deoxygenated sample of 1,8-nonadiyne. The silicon sample was then kept under nitrogen for 2 h at a distance of approximately 200 mm from a 312 nm UV source (Vilber, VL-215.M). The chemically passivated silicon electrodes were rinsed with dichloromethane, rested for 24 h in a sealed vial under dichloromethane at +4 °C, and then blown dry under a nitrogen stream before being analyzed. The silicon electrodes were mounted in a three-electrode and single-compartment polytetrafluoroethylene (PTFE) custom cell where a circular Viton gasket defined the geometric area of the working electrode to 0.28 cm^2. Ohmic contact between the back of the silicon sample and a copper plate was achieved by gently scribing the back of the electrode with emery paper before applying on it a small amount of gallium−indium eutectic. The topography of both silicon and carbon samples was estimated before the electrochemical experiments by atomic force microscopy (AFM). AFM data were acquired on a Park NX10 (Park Systems Corporation, Suwon, Korea). The scanning was conducted in True Non-Contact™ mode. The silicon sample was fixed on a steel plate using carbon tape, and then mounted on the AFM magnetic sample holder. Imaging was done in air, at room temperature, using n-type silicon AFM probes (OCML-AC160TS, Olympus Corporation, Tokyo, Japan) with a nominal resonance frequency of 300 kHz and a spring constant of 26 N/m. The image size was set to 5 × 5 μm, the resolution to 256 points/line, and the scan rate to 1Hz (Supporting Information, Figures S22 and S23). Prior to the OCP−time measurements, electrodes were left to equilibrate in contact with the ionic liquid sample until the first derivative of the OCP versus time traces (dV/dt) dropped below |0.0001|. This was normally achieved within five minutes of immersing the electrodes in the liquid (Supporting Information, Figures S24–S27). After this initial stabilization phase, a potential step of variable magnitude and sign was applied to the working electrode. Unless specified otherwise the duration of this potential pulse was 60 s. OCP recording was resumed immediately after the pulse. The time that elapsed between the anodic, or cathodic, excursion and the resuming of the OCP measurement was less than 2 s.

Computational Methods. The CL&Pol[77-79] force field optimized for ionic liquids was enforced on periodic simulation boxes containing 125 ion pairs of [BMIM][PF_6], [HMIM][PF_6] and [EMIM][$EtSO_4$]. Where necessary, k_{ij} parameters were calculated (See Supporting Information Table S1). All systems had initial structures produced with PACKMOL,[80] and were initially equilibrated for 5 ns in an NpT ensemble, proving to be ample time for each system's density to converge (Supporting Information, Figure S28). Average densities from the last nanosecond of equilibration were within 5% of experimental values (see Supporting Information, Table S2), with corresponding average volumes enforced for 10 ns NVT production runs. Separate NVT runs from identical restart files were performed, with the absence or presence of a 0.2 V/Å external field along the positive z-axis direction. Initially, all systems were allowed 0.1 ns to deform to the average box volume, and a further picosecond to align with the electric field where necessary before the production run. In all simulations, Nose-Hoover temperature grouped thermostats and barostats were used, with atoms thermalized to 353 K and drude particles thermalized to 1 K, and a 1 fs timestep was used in all simulations. The LAMMPS[81] software package was used to run all simulations, utilizing the USER-DRUDE module. Trajectory analysis was performed using TRAVIS[82-83] software, with dipole moments calculated with force field charges, and each ion's centre of mass as a reference point. The magnitude of these calculated dipole moments are also known as the ion's 'charge arm.' Volume of cations was calculated based on the previously published methodology.[66] The volume for $EMIM^+$ was taken from that work[66] and the volumes of $BMIM^+$ and $HMIM^+$ cations are given in Supporting Information, Table S5. The diffusion coefficients were measured as the slope of the mean standard deviation (MSD) of each ion's centre of mass. All contributions of each ion across the production runs were considered, with maximum correlation times set to 30% of the trajectory. Correlation times of 1.5 to 3.0 ns were sampled, and produced linear fits of correlation coefficients of at least 0.99 in all cases. These analyses were performed with TRAVIS.

ASSOCIATED CONTENT

PDF file containing electrochemical and OCP data, atomic force microscopy data, experimental and simulated cyclic voltammograms and supplementary computational results. Zipped XYZ files containing snapshots of the MD simulations. The Supporting Information is available free of charge at on the ACS Publications website.

AUTHOR INFORMATION

Corresponding Authors

Michelle L. Coote − ARC Centre of Excellence for Electromaterials Science, Research School of Chemistry, Australian National University, Canberra, Australian Capital Territory 2601, Australia; orcid.org/0000-0003-0828-7053; Email: michelle.coote@anu.edu.au

Simone Ciampi − School of Molecular and Life Sciences, Curtin University, Bentley, Western Australia 6102, Australia; orcid.org/0000-0002-8272-8454; Email: simone.ciampi@curtin.edu.au

Ekaterina I. Izgorodina – School of Chemistry, Monash University, Clayton, VIC 3800, Australia; orcid.org/0000-0002-2506-4890; Email: katya.pas@monash.edu

Authors

Mattia Belotti – School of Molecular and Life Sciences, Curtin University, Bentley, Western Australia 6102, Australia; orcid.org/0000-0002-7382-337X

Xin Lyu – School of Molecular and Life Sciences, Curtin University, Bentley, Western Australia 6102, Australia; orcid.org/0000-0002-6506-0392

Longkun Xu – ARC Centre of Excellence for Electromaterials Science, Research School of Chemistry, Australian National

University, Canberra, Australian Capital Territory 2601, Australia; orcid.org/0000-0001-7314-2913

Peter Halat – School of Chemistry, Monash University, Clayton, VIC 3800, Australia; orcid.org/0000-0002-0878-6963

Nadim Darwish – School of Molecular and Life Sciences, Curtin University, Bentley, Western Australia 6102, Australia; orcid.org/0000-0002-6565-1723

Debbie S. Silvester – School of Molecular and Life Sciences, Curtin University, Bentley, Western Australia 6102, Australia; orcid.org/0000-0002-7678-7482

Author Contributions

The manuscript was written through contributions of all the authors. All authors have given approval to the final version of the manuscript.

Notes

The authors declare no competing financial interests.

ACKNOWLEDGMENTS

This work was financially supported by the Australian Research Council (DP190100735 and FT190100148 (S.C.), and FL170100041 (M.L.C.)).

REFERENCES

(1) Barrosse-Antle, L. E.; Bond, A. M.; Compton, R. G.; O'Mahony, A. M.; Rogers, E. I.; Silvester, D. S., Voltammetry in Room Temperature Ionic Liquids: Comparisons and Contrasts with Conventional Electrochemical Solvents. *Chem. Asian J.* **2010,** *5*, 202–230.

(2) Ghandi, K., A Review of Ionic Liquids, Their Limits and Applications. *Green and Sustainable Chem.* **2013,** *04*, 44–53.

(3) Gabriel, S.; Weiner, J., Ueber Einige Abkömmlinge Des Propylamins. *Berichte der deutschen chemischen Gesellschaft* **1888,** *21*, 2669–2679.

(4) Bonhôte, P.; Dias, A.-P.; Papageorgiou, N.; Kalyanasundaram, K.; Grätzel, M., Hydrophobic, Highly Conductive Ambient-Temperature Molten Salts. *Inorg. Chem.* **1996,** *35*, 1168–1178.

(5) De Vos, N.; Maton, C.; Stevens, C. V., Electrochemical Stability of Ionic Liquids: General Influences and Degradation Mechanisms. *Chem. Electro. Chem.* **2014,** *1*, 1258–1270.

(6) Zhong, C.; Deng, Y.; Hu, W.; Qiao, J.; Zhang, L.; Zhang, J., A Review of Electrolyte Materials and Compositions for Electrochemical Supercapacitors. *Chem. Soc. Rev.* **2015,** *44*, 7484–7539.

(7) Wu, J.; Lan, Z.; Lin, J.; Huang, M.; Huang, Y.; Fan, L.; Luo, G., Electrolytes in Dye-Sensitized Solar Cells. *Chem. Rev.* **2015,** *115*, 2136–2173.

(8) Osada, I.; de Vries, H.; Scrosati, B.; Passerini, S., Ionic-Liquid-Based Polymer Electrolytes for Battery Applications. *Angew. Chem. Int. Ed.* **2016,** *55*, 500–513.

(9) Watanabe, M.; Thomas, M. L.; Zhang, S.; Ueno, K.; Yasuda, T.; Dokko, K., Application of Ionic Liquids to Energy Storage and Conversion Materials and Devices. *Chem. Rev.* **2017,** *117*, 7190–7239.

(10) Li, H.; Kobrak, M. N., A Molecular Dynamics Study of the Influence of Ionic Charge Distribution on the Dynamics of a Molten Salt. *J. Chem. Phys.* **2009,** *131*, 194507.

(11) Gebbie, M. A.; Valtiner, M.; Banquy, X.; Fox, E. T.; Henderson, W. A.; Israelachvili, J. N., Ionic Liquids Behave as Dilute Electrolyte Solutions. *Proc. Natl. Acad. Sci.* **2013,** *110*, 9674–9679.

(12) Perkin, S.; Salanne, M.; Madden, P.; Lynden-Bell, R., Is a Stern and Diffuse Layer Model Appropriate to Ionic Liquids at Surfaces? *Proc. Natl. Acad. Sci.* **2013,** *110*, E4121–E4121.

(13) Welton, T., Room-Temperature Ionic Liquids. Solvents for Synthesis and Catalysis. *Chem. Rev.* **1999,** *99*, 2071–2084.

(14) Hallett, J. P.; Welton, T., Room-Temperature Ionic Liquids: Solvents for Synthesis and Catalysis. 2. *Chem. Rev.* **2011,** *111*, 3508–3576.

(15) Krossing, I.; Slattery, J. M.; Daguenet, C.; Dyson, P. J.; Oleinikova, A.; Weingärtner, H., Why Are Ionic Liquids Liquid? A Simple Explanation Based on Lattice and Solvation Energies. *J. Am. Chem. Soc.* **2006,** *128*, 13427–13434.

(16) Gong, X.; Kozbial, A.; Li, L., What Causes Extended Layering of Ionic Liquids on the Mica Surface? *Chem. Sci.* **2015,** *6*, 3478–3482.

(17) Mezger, M.; Schröder, H.; Reichert, H.; Schramm, S.; Okasinski, J. S.; Schöder, S.; Honkimäki, V.; Deutsch, M.; Ocko, B. M.; Ralston, J.; Rohwerder, M.; Stratmann, M.; Dosch, H., Molecular Layering of Fluorinated Ionic Liquids at a Charged Sapphire (0001) Surface. *Science* **2008,** *322*, 424–428.

(18) Yamamoto, R.; Morisaki, H.; Sakata, O.; Shimotani, H.; Yuan, H.; Iwasa, Y.; Kimura, T.; Wakabayashi, Y., External Electric Field Dependence of the Structure of the Electric Double Layer at an Ionic Liquid/Au Interface. *Appl. Phys. Lett.* **2012,** *101*, 053122.

(19) Perkin, S.; Crowhurst, L.; Niedermeyer, H.; Welton, T.; Smith, A. M.; Gosvami, N. N., Self-Assembly in the Electrical Double Layer of Ionic Liquids. *Chem. Comm.* **2011,** *47*, 6572–6574.

(20) Fedorov, M. V.; Kornyshev, A. A., Ionic Liquids at Electrified Interfaces. *Chem. Rev.* **2014,** *114*, 2978–3036.

(21) Li, H.; Rutland, M. W.; Atkin, R., Ionic Liquid Lubrication: Influence of Ion Structure, Surface Potential and Sliding Velocity. *Phys. Chem. Chem. Phys.* **2013,** *15*, 14616–14623.

(22) Sha, M.; Wu, G.; Dou, Q.; Tang, Z.; Fang, H., Double-Layer Formation of [Bmim][Pf6] Ionic Liquid Triggered by Surface Negative Charge. *Langmuir* **2010,** *26*, 12667–12672.

(23) Nishi, N.; Uchiyashiki, J.; Ikeda, Y.; Katakura, S.; Oda, T.; Hino, M.; Yamada, N. L., Potential-Dependent Structure of the Ionic Layer at the Electrode Interface of an Ionic Liquid Probed Using Neutron Reflectometry. *J. Phys. Chem. C* **2019,** *123*, 9223–9230.

(24) Zhang, X.; Zhong, Y.-X.; Yan, J.-W.; Su, Y.-Z.; Zhang, M.; Mao, B.-W., Probing Double Layer Structures of Au (111)–Bmipf6 Ionic Liquid Interfaces from Potential-Dependent Afm Force Curves. *Chem. Comm.* **2012,** *48*, 582–584.

(25) Gebbie, M. A.; Dobbs, H. A.; Valtiner, M.; Israelachvili, J. N., Long-Range Electrostatic Screening in Ionic Liquids. *Proc. Natl. Acad. Sci.* **2015,** *112*, 7432–7437.

(26) Bazant, M. Z.; Storey, B. D.; Kornyshev, A. A., Double Layer in Ionic Liquids: Overscreening Versus Crowding. *Phys. Rev. Lett.* **2011,** *106*, 046102.

(27) Li, H.; Endres, F.; Atkin, R., Effect of Alkyl Chain Length and Anion Species on the Interfacial Nanostructure of Ionic Liquids at the Au(111)–Ionic Liquid Interface as a Function of Potential. *Phys. Chem. Chem. Phys.* **2013,** *15*, 14624–14633.

(28) Bozzini, B.; Busson, B.; Humbert, C.; Mele, C.; Raffa, P.; Tadjeddine, A., Investigation of Au Electrodeposition from [Bmp][Tfsa] Room-Temperature Ionic Liquid Containing K[Au(Cn)2] by in Situ Two-Dimensional Sum Frequency Generation Spectroscopy. *J. Electroanal. Chem.* **2011,** *661*, 20–24.

(29) Atkin, R.; Warr, G. G., Structure in Confined Room-Temperature Ionic Liquids. *J. Phys. Chem. C* **2007,** *111*, 5162–5168.

(30) Toda, S.; Clark, R.; Welton, T.; Shigeto, S., Observation of the Pockels Effect in Ionic Liquids and Insights into the Length Scale of Potential-Induced Ordering. *Langmuir* **2021,** *37*, 5193–5201.

(31) Arzhantsev, S.; Jin, H.; Ito, N.; Maroncelli, M., Observing the Complete Solvation Response of Dcs in Imidazolium Ionic Liquids, from the Femtosecond to Nanosecond Regimes. *Chem. Phys. Lett.* **2006,** *417*, 524–529.

(32) Nishi, N.; Hirano, Y.; Motokawa, T.; Kakiuchi, T., Ultraslow Relaxation of the Structure at the Ionic Liquid|Gold Electrode Interface to a Potential Step Probed by Electrochemical Surface Plasmon Resonance Measurements: Asymmetry of the Relaxation Time to the Potential-Step Direction. *Phys. Chem. Chem. Phys.* **2013,** *15*, 11615–11619.

(33) Roling, B.; Drüschler, M.; Huber, B., Slow and Fast Capacitive Process Taking Place at the Ionic Liquid/Electrode Interface. *Faraday Discuss.* **2012,** *154*, 303–311.

(34) Zhou, W.; Xu, Y.; Ouchi, Y., Hysteresis Effects in the in Situ Sfg and Differential Capacitance Measurements on Metal Electrode/Ionic Liquids Interface. *ECS Trans.* **2013,** *50*, 339–348.

(35) Makino, S.; Kitazumi, Y.; Nishi, N.; Kakiuchi, T., Charging Current Probing of the Slow Relaxation of the Ionic Liquid Double Layer at the Pt Electrode. *Electrochem. Commun.* **2011,** *13*, 1365–1368.

(36) Fedorov, M. V.; Kornyshev, A. A., Ionic Liquid near a Charged Wall: Structure and Capacitance of Electrical Double Layer. *J. Phys. Chem. B* **2008,** *112*, 11868–11872.

(37) Baldelli, S., Probing Electric Fields at the Ionic Liquid−Electrode Interface Using Sum Frequency Generation Spectroscopy and Electrochemistry. *J. Phys. Chem. B* **2005,** *109*, 13049–13051.

(38) Baldelli, S., Surface Structure at the Ionic Liquid−Electrified Metal Interface. *Acc. Chem. Res.* **2008,** *41*, 421–431.

(39) Alam, M. T.; Islam, M. M.; Okajima, T.; Ohsaka, T., Measurements of Differential Capacitance at Mercury/Room-Temperature Ionic Liquids Interfaces. *J. Phys. Chem. C* **2007,** *111*, 18326-–18333.
(40) Uysal, A.; Zhou, H.; Feng, G.; Lee, S. S.; Li, S.; Fenter, P.; Cummings, P. T.; Fulvio, P. F.; Dai, S.; McDonough, J. K.; Gogotsi, Y., Structural Origins of Potential Dependent Hysteresis at the Electrified Graphene/Ionic Liquid Interface. *J. Phys. Chem. C* **2014,** *118*, 569–574.
(41) Kornyshev, A. A., Double-Layer in Ionic Liquids: Paradigm Change? *J. Phys. Chem. B* **2007,** *111*, 5545–5557.
(42) Rivera-Rubero, S.; Baldelli, S., Surface Spectroscopy of Room-Temperature Ionic Liquids on a Platinum Electrode: A Sum Frequency Generation Study. *J. Phys. Chem. B* **2004,** *108*, 15133–15140.
(43) Lockett, V.; Sedev, R.; Ralston, J.; Horne, M.; Rodopoulos, T., Differential Capacitance of the Electrical Double Layer in Imidazolium-Based Ionic Liquids: Influence of Potential, Cation Size, and Temperature. *J. Phys. Chem. C* **2008,** *112*, 7486–7495.
(44) Aliaga, C.; Baldelli, S., Sum Frequency Generation Spectroscopy and Double-Layer Capacitance Studies of the 1-Butyl-3-Methylimidazolium Dicyanamide−Platinum Interface. *J. Phys. Chem. B* **2006,** *110*, 18481–18491.
(45) Jurado, L. A.; Espinosa-Marzal, R. M., Insight into the Electrical Double Layer of an Ionic Liquid on Graphene. *Sci. Rep.* **2017,** *7*, 4225.
(46) Brandt, A.; Pohlmann, S.; Varzi, A.; Balducci, A.; Passerini, S., Ionic Liquids in Supercapacitors. *MRS Bulletin* **2013,** *38*, 554–559.
(47) Salanne, M., Ionic Liquids for Supercapacitor Applications. In *Ionic Liquids Ii*, Kirchner, B.; Perlt, E., Eds. Springer International Publishing: Cham, 2018; pp 29–53.
(48) Ramaswamy, N.; Mukerjee, S., Influence of Inner- and Outer-Sphere Electron Transfer Mechanisms During Electrocatalysis of Oxygen Reduction in Alkaline Media. *J. Phys. Chem. C* **2011,** *115*, 18015–18026.
(49) Bhat, M. A.; Ingole, P. P.; Chaudhari, V. R.; Haram, S. K., Outer Sphere Electroreduction of Ccl4 in 1-Butyl-3-Methylimmidazolium Tetrafluoroborate: An Example of Solvent Specific Effect of Ionic Liquid. *J. Phys. Chem. B* **2009,** *113*, 2848–2853.
(50) Xu, L.; Izgorodina, E. I.; Coote, M. L., Ordered Solvents and Ionic Liquids Can Be Harnessed for Electrostatic Catalysis. *J. Am. Chem. Soc.* **2020,** *142*, 12826-12833.
(51) Shaik, S.; Mandal, D.; Ramanan, R., Oriented Electric Fields as Future Smart Reagents in Chemistry. *Nat. Chem.* **2016,** *8*, 1091-1098.
(52) Meir, R.; Chen, H.; Lai, W.; Shaik, S., Oriented Electric Fields Accelerate Diels-Alder Reactions and Control the Endo/Exo Selectivity. *Chem. phys. chem.* **2010,** *11*, 301–310.
(53) Shaik, S.; Ramanan, R.; Danovich, D.; Mandal, D., Structure and Reactivity/Selectivity Control by Oriented-External Electric Fields. *Chem. Soc. Rev.* **2018,** *47*, 5125–5145.
(54) Ciampi, S.; Darwish, N.; Aitken, H. M.; Díez-Pérez, I.; Coote, M. L., Harnessing Electrostatic Catalysis in Single Molecule, Electrochemical and Chemical Systems: A Rapidly Growing Experimental Tool Box. *Chem. Soc. Rev.* **2018,** *47*, 5146-5164.
(55) Fedorov, M. V.; Kornyshev, A. A., Towards Understanding the Structure and Capacitance of Electrical Double Layer in Ionic Liquids. *Electrochim. Acta* **2008,** *53*, 6835–6840.
(56) Gooding, J. J.; Ciampi, S., The Molecular Level Modification of Surfaces: From Self-Assembled Monolayers to Complex Molecular Assemblies. *Chem. Soc. Rev.* **2011,** *40*, 2704-2718.
(57) Fedorov, M. V.; Georgi, N.; Kornyshev, A. A., Double Layer in Ionic Liquids: The Nature of the Camel Shape of Capacitance. *Electrochem. Commun.* **2010,** *12*, 296–299.
(58) Hayes, R.; Borisenko, N.; Tam, M. K.; Howlett, P. C.; Endres, F.; Atkin, R., Double Layer Structure of Ionic Liquids at the Au(111) Electrode Interface: An Atomic Force Microscopy Investigation. *J. Phys. Chem. C* **2011,** *115*, 6855–6863.
(59) Peart, R. F., Self Diffusion in Intrinsic Silicon. *Physica Status Solidi (b)* **1966,** *15*, K119–K122.
(60) Gomes, C.; Costa, R.; Pereira, C. M.; Silva, A. F., The Electrical Double Layer at the Ionic Liquid/Au and Pt Electrode Interface. *RSC Adv.* **2014,** *4*, 28914–28921.
(61) Alonso, C.; Salvarezza, R. C.; Vara, J. M.; Arvia, A. J.; Vazquez, L.; Bartolome, A.; Baro, A. M., The Evaluation of Surface Diffusion Coefficients of Gold and Platinum Atoms at Electrochemical Interfaces from Combined Stm-Sem Imaging and Electrochemical Techniques. *J. Electrochem. Soc.* **1990,** *137*, 2161–2166.
(62) Low, K.; Wylie, L.; Scarborough, D. L. A.; Izgorodina, E. I., Is It Possible to Control Kinetic Rates of Radical Polymerisation in Ionic Liquids? *Chem. Commun.* **2018,** *54*, 11226–11243.
(63) Kobrak, M. N.; Sandalow, N., An Electrostatic Interpretation of Structure-Property Relationships in Ionic Liquids. *ECS Proceedings Volumes* **2004,** *2004-24*, 417.
(64) Clark, R.; von Domaros, M.; McIntosh, A. J. S.; Luzar, A.; Kirchner, B.; Welton, T., Effect of an External Electric Field on the Dynamics and Intramolecular Structures of Ions in an Ionic Liquid. *J. Chem. Phys.* **2019,** *151*, 164503.
(65) Rigby, J.; Izgorodina, E. I., New Scs- and Sos-Mp2 Coefficients Fitted to Semi-Coulombic Systems. *J. Chem. Theory Comput.* **2014,** *10*, 3111–3122.
(66) Izgorodina, E. I.; Forsyth, M.; MacFarlane, D. R., On the Components of the Dielectric Constants of Ionic Liquids: Ionic Polarization? *Phys. Chem. Chem. Phys.* **2009,** *11*, 2452–2458.
(67) Aragonès, A.; Haworth, N.; Darwish, N.; Ciampi, S.; Bloomfield, N.; Wallace, G.; Diez-Perez, I.; Coote, M., Electrostatic Catalysis of a Diels–Alder Reaction. *Nature* **2016,** *531*, 88–91.
(68) Zhang, L.; Laborda, E.; Darwish, N.; Noble, B. B.; Tyrell, J. H.; Pluczyk, S.; Le Brun, A. P.; Wallace, G. G.; Gonzalez, J.; Coote, M. L.; Ciampi, S., Electrochemical and Electrostatic Cleavage of Alkoxyamines. *J. Am. Chem. Soc.* **2018,** *140*, 766–774.
(69) Evanko, B.; Boettcher, S. W.; Yoo, S. J.; Stucky, G. D., Redox-Enhanced Electrochemical Capacitors: Status, Opportunity, and Best Practices for Performance Evaluation. *ACS Energy Lett.* **2017,** *2*, 2581–2590.
(70) Mourad, E.; Coustan, L.; Lannelongue, P.; Zigah, D.; Mehdi, A.; Vioux, A.; Freunberger, S. A.; Favier, F.; Fontaine, O., Biredox Ionic Liquids with Solid-Like Redox Density in the Liquid State for High-Energy Supercapacitors. *Nat. Mater.* **2017,** *16*, 446–453.
(71) Gale, R. J.; Osteryoung, R. A., The Electrical Double Layer at Mercury in Room Temperature Aluminum Chloride: 1-Butylpyridinium Chloride Ionic Liquids. *Electrochim. Acta* **1980,** *25*, 1527–1529.
(72) Lockett, V.; Horne, M.; Sedev, R.; Rodopoulos, T.; Ralston, J., Differential Capacitance of the Double Layer at the Electrode/Ionic Liquids Interface. *Phys. Chem. Chem. Phys.* **2010,** *12*, 12499–12512.
(73) Graves, A. D.; Inman, D., Adsorption and the Differential Capacitance of the Electrical Double-Layer at Platinum/Halide Metal Interfaces. *Nature* **1965,** *208*, 481–482.
(74) Ciampi, S.; Böcking, T.; Kilian, K. A.; James, M.; Harper, J. B.; Gooding, J. J., Functionalization of Acetylene-Terminated Monolayers on Si(100) Surfaces: A Click Chemistry Approach. *Langmuir* **2007,** *23*, 9320–9329.
(75) Zhang, L.; Vogel, Y. B.; Noble, B. B.; Gonçales, V. R.; Darwish, N.; Brun, A. L.; Gooding, J. J.; Wallace, G. G.; Coote, M. L.; Ciampi, S., Tempo Monolayers on Si(100) Electrodes: Electrostatic Effects by the Electrolyte and Semiconductor Space-Charge on the Electroactivity of a Persistent Radical. *J. Am. Chem. Soc.* **2016,** *138*, 9611–9619.
(76) Ferrie, S.; Darwish, N.; Gooding, J. J.; Ciampi, S., Harnessing Silicon Facet-Dependent Conductivity to Enhance the Direct-Current Produced by a Sliding Schottky Diode Triboelectric Nanogenerator. *Nano Energy* **2020,** *78*, 105210.
(77) Canongia Lopes, J. N.; Deschamps, J.; Pádua, A. A. H., Modeling Ionic Liquids Using a Systematic All-Atom Force Field. *J. Phys. Chem. B* **2004,** *108*, 2038–2047.
(78) Canongia Lopes, J. N.; Pádua, A. A. H.; Shimizu, K., Molecular Force Field for Ionic Liquids Iv: Trialkylimidazolium and Alkoxycarbonyl-Imidazolium Cations; Alkylsulfonate and Alkylsulfate Anions. *J. Phys. Chem. B* **2008,** *112*, 5039–5046.
(79) Goloviznina, K.; Canongia Lopes, J. N.; Costa Gomes, M.; Pádua, A. A. H., Transferable, Polarizable Force Field for Ionic Liquids. *J. Chem. Theory Comput.* **2019,** *15*, 5858–5871.
(80) Martínez, L.; Andrade, R.; Birgin, E. G.; Martínez, J. M., Packmol: A Package for Building Initial Configurations for Molecular Dynamics Simulations. *J. Comput. Chem.* **2009,** *30*, 2157–2164.
(81) Plimpton, S., Fast Parallel Algorithms for Short-Range Molecular Dynamics. *J. Comput. Phys.* **1995,** *117*, 1–19.
(82) Brehm, M.; Kirchner, B., Travis - a Free Analyzer and Visualizer for Monte Carlo and Molecular Dynamics Trajectories. *J. Chem. Inf. Model.* **2011,** *51*, 2007–2023.
(83) Brehm, M.; Thomas, M.; Gehrke, S.; Kirchner, B., Travis—a Free Analyzer for Trajectories from Molecular Simulation. *J. Chem. Phys.* **2020,** *152*, 164105.

Insert Table of Contents artwork here